Modulation of absorption manner in helicon discharges by changing profile of low axial magnetic field*

Gao Zhao(赵高)[1], Yu Wang(王宇)[1], Chen Niu(牛晨)[2], Zhong-Wei Liu(刘忠伟)[2], Jiting Ouyang(欧阳吉庭)[1,†], and Qiang Chen(陈强)[2,‡]

[1] School of Physics, Beijing Institute of Technology, Beijing 100081, China
[2] Laboratory of Plasma Physics & Materials, Beijing Institute of Graphic Communication, Beijing 102600, China

(Received 5 May 2017; revised manuscript received 15 June 2017; published online 20 August 2017)

The modulation of absorption manner in helicon discharge by changing the profile of low axial magnetic field is explored experimentally in this work. The experiments are carried out in Boswell-type antenna driven by 13.56-MHz power source in 0.35-Pa argon environment. The peak of the external non-uniform magnetic field (B_{ex}) along the axis is observed in a range from 0 Gs to 250 Gs (1 Gs = 10^{-4} T), where the electron density varies from 0.5×10^{16} m^{-3} to 9×10^{16} m^{-3}. When B_{ex} is located near the tube upper end sealed by a dielectric plate, or near the tube bottom end connected with a diffusion chamber, the plasmas are centralized in the tube in the former case while the strong luminance appears between the edge of the tube and the axial line in the latter case. When B_{ex} is located in the middle of the antenna, moreover, an effective resistance (R_{eff}) peak appears apparently with increasing magnetic field. The glow moves toward first the edge of the tube and then the two antenna legs as the magnetic field increases. The discharge in this case is caused by the absorption of Trivelpiece–Gould (TG) wave. It is suggested that B_{ex} is located in the middle of the antenna to obtain a higher efficiency of power transfer.

Keywords: helicon discharge, absorption manner, low supply power, low axial magnetic field

PACS: 52.50.Qt, 52.40.Db **DOI:** 10.1088/1674-1056/26/10/105201

1. Introduction

Helicon discharge was first introduced by Boswell in 1970,[1] which demonstrates a high ionization efficiency with an electron density in a range of 10^{17} m^{-3}–10^{20} m^{-3}. Recently, helicon plasma has increasingly received attention in the plasma thruster field.[1,2] They are generally right-handed polarized waves and correspond to whistler waves in a radially unbounded plasma, especially in low magnetic field. However, in a bounded geometry, both right-handed polarized and left-handed polarized waves can exist, even though the right-handed polarized waves are always preferentially excited.[3] In most cases, it is thought that the helicon wave and the Trivelpiece–Gould (TG) wave will simultaneously appear in a helicon discharge system.[3,4]

When Chen *et al.*[5] characterized the helicon plasma along with the increase of external magnetic field, they noticed that a density peak appeared in a low magnetic field range (from 20 Gs to 50 Gs), which then has also been noticed by several other groups.[6–15] In recent years, the multiple low-field density peaks were reported.[14,16] Helicon plasma generated in a non-uniform magnetic field was also addressed in previous research.[17–19] For example, Virko *et al.*[20] examined the plasma characteristics and wave structures in $m = 0$ helicon discharge operated in a non-uniform magnetic field. Their investigations focused on the comparison between the cases of uniform and non-uniform magnetic field at high RF supply power ($\sim$ 1.1 kW). They found that the electron density increases with the increase of magnetic field gradient in the antenna region compared with the scenario in the uniform magnetic field. The directional and extended power deposition together with high electron conductivity along the magnetic lines was employed to explain the generation of hot electrons and enhanced plasma production in the gradient magnetic field.[20] Lafleur *et al.*[21] mentioned that the density distribution in the axial direction was significantly affected by axial magnetic field profile. They considered that the plasma was confined by the magnetic field, and forced to undergo expansion as the field diverges. Takahashi *et al.*[22] found the plasma was more preferential to gather around the axis of the plasma column after installing a permanent magnet (PM) behind the substrate, which was located downstream of the source exit. They thought that PM plays a role in constricting the plasma rather than in improving the plasma production. Also, they found the standing wave can be induced by a rapidly bent magnetic field,[23] and the standing wave was generated due to a spatially localized change of a plasma refractive index. All these results indicate that the helicon discharge is greatly relevant to the magnetic field profile. Therefore, the investigation

*Project supported by the National Natural Science Foundation of China (Grant Nos. 11175024, 11375031, and 11505013), the Beijing Natural Science Foundation of China (Grant No. KZ201510015014), and the Beijing Municipal Natural Science Foundation, China (Grant No. 4162024).

†Corresponding author. E-mail: jtouyang@bit.edu.cn
‡Corresponding author. E-mail: lppmchenqiang@hotmail.com

© 2017 Chinese Physical Society and IOP Publishing Ltd

of the effects of different low axial magnetic field profile on discharge was indispensable.

In this work, we investigate experimentally the helicon plasma in different low axial magnetic field profiles at a low supply power. We find that the absorption manner in helicon discharge can be modulated efficiently by changing the profile of the axial magnetic field.

2. Experimental setup and diagnostics

The experimental setup is shown schematically in Fig. 1, which has been described in detail elsewhere.[16] Briefly, the discharge system consists of a quartz cylinder (34 cm in length and 7 cm in inner diameter) with one end connected to a diffusion chamber (30 cm in length and 33 cm in inner diameter), and the other end of the tube is sealed by a dielectric plate (polytetrafluoroethylene, PTFE). The discharge gas is pure argon at a pressure of 0.35 Pa. The neutral gas pressure is measured with a vacuum gauge attached to the end of the diffusion chamber. A double-saddle field antenna (noted as Boswell type antenna[24]) of 15.5 cm in length surrounds the source tube and is powered by a 13.56-MHz RF generator with power increasing up to 10 kW.

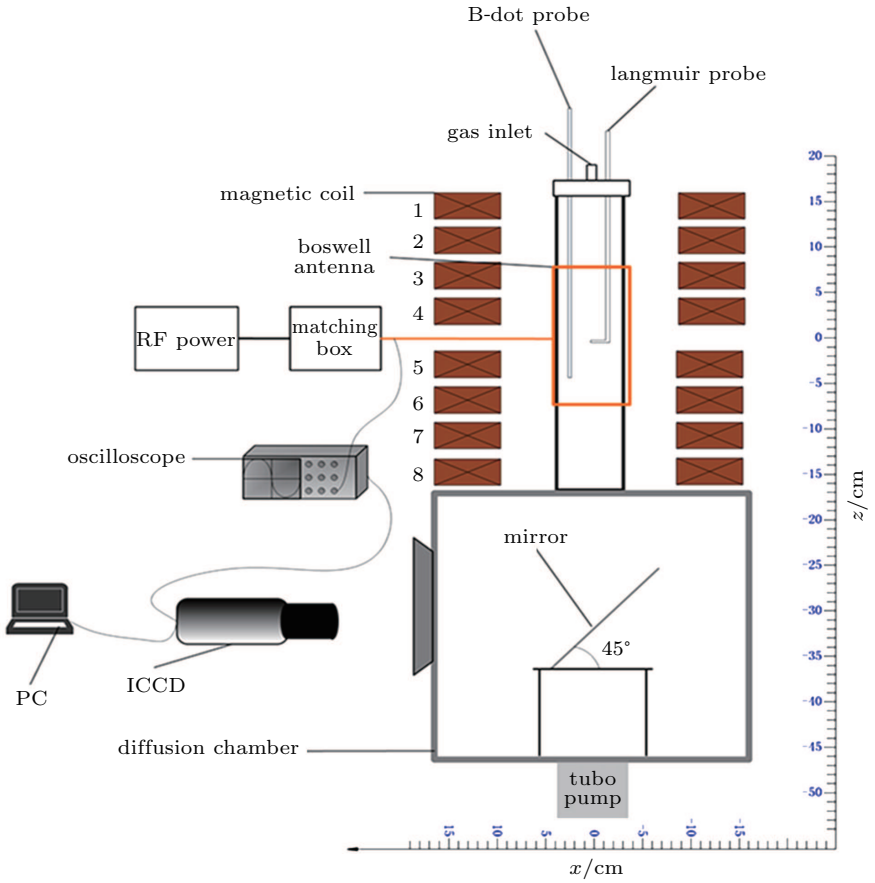


Fig. 1. (color online) Schematic diagram of experimental setup.

The discharge characteristics are investigated in different profiles of low magnetic field controlled through turning on/off the magnetic coils at different positions. Figure 2 shows three kinds of magnetic field profiles used in this work: (a) Case 1: coils 1#, 2# (in Fig. 1(a)) turn on, and the others are off; (b) Case 2: coils 3#, 4#, 5#, and 6# are on and the others are off; And (c) Case 3: coils 7# and 8# are on and the others are off. The direction of B_{ex} in axial line points to the diffusion chamber. The simulated magnetic fields are also plotted based on using COMSOL software simulation. The zero of the Z axis is set to be in the middle of the antenna with the negative Z axis being towards the diffusion chamber and the positive one being towards the end plate.

Electron density is measured by using an ALP System™RF compensated Langmuir single probe (Impedans, UK). The wire diameter and exposed length of the probe are 0.1 mm and 6 mm, respectively. A B-dot can only detect the dynamic electromagnetic signal according to Faraday's law and it cannot pick up the value of static external magnetic field. This makes sure that the magnetic component B_z of electromagnetic signals in Z axis and the phase angle of helicon wave are measured by an RF B-dot magnetic probe consisting of a coaxial cable and a 4-turn insulated copper wire coil wound on a quartz bobbin (2 mm in outer diameter (O.D.)). This B-dot was calibrated in a Helmholtz coil with two one-turn loops, which generated the test RF mag-

netic field, and a center-trapped transformer (CTT) was also used to reduce the capacitive coupling noise. Detailed design of this probe can be seen in Ref. [25]. The discharge images are taken by a high speed ICCD (Princeton Instruments MAX2) with an exposure time of 2 ns to investigate the discharge mode transition. Each picture was an accumulation of 100 shots at the same time in a period when the discharge is in a stable state. A telephoto lens (Nikon AF NIKKOR, 700 mm–300 mm) was used in experiment. The depth of focus in our experiment was about 33 cm. For a good repeatability and continuity the ICCD images were the same in time when the discharge was stable. The images shown in this paper correspond to 1/8 RF period. The discharge current was recorded by a digital oscilloscope (Tektronix DPO4104) with a Rogowski coil (resolution, 1 μA). The forward RF power could be obtained from the power-meter of RF power supply and its match box. The input powers were obtained through the data measured by RF current and voltage probes. The effective resistance $R_{\rm eff}$ was calculated from $R_{\rm eff} = P/I_{\rm rms}^2$ (where P is the input power and $I_{\rm rms}$ is the root-mean-square current). Since the reflective power was generally smaller than 1% of the incident power in experiment, the input power was nearly equal to the forward power.

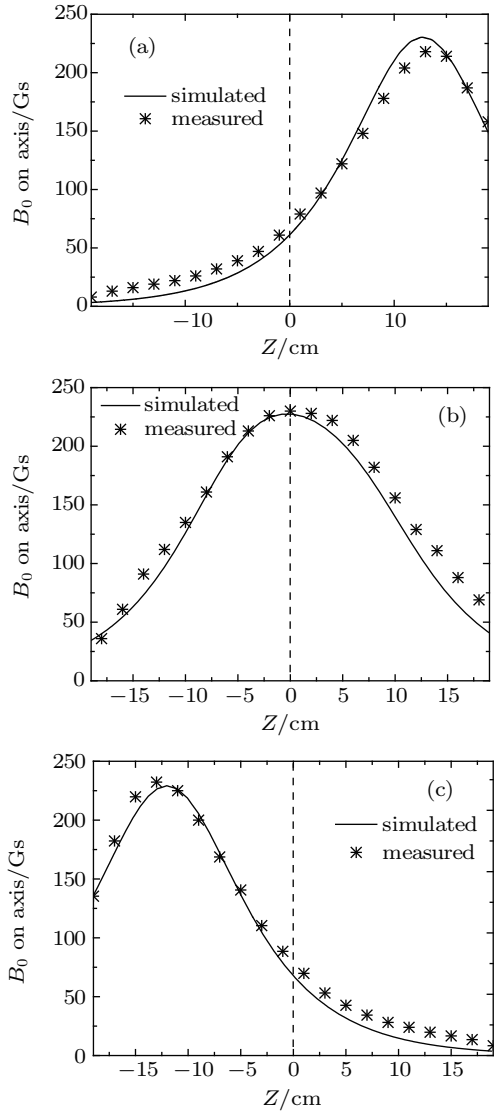


Fig. 2. Three kinds of magnetic field profiles used in this work. (a) Case 1: coils 1#, 2# are on, the other coils are off; (b) Case 2: coils 3#, 4#, 5#, and 6# are on, the other ones are off; (c) Case 3: coils 7# and 8# are on, the other ones are off.

3. Experimental results

3.1. Case 1: $B_{\rm ex}$ located near the dielectric end plate

The end-view ICCD images at increasing magnetic field along Z axis ($B_{\rm ex}$) in Case 1 are shown in Fig. 3. The input power is 140 W. It is seen that the discharge tends to be centralized at the axis with increasing $B_{\rm ex}$. The higher the magnetic field, the smaller the radius of the strong luminance region and the brighter the glow near the central axis. Since the luminous distribution of the discharge is generally consistent with the distribution of power deposition,[16] we use this luminous distribution to evaluate the plasma state.

The effective resistance in Case 1, on the other hand, does not show an apparent variation with the $B_{\rm ex}$ increasing. This bulk absorption seems to be caused by helicon wave (e.g., Chen[26] and Ganguli[27]).

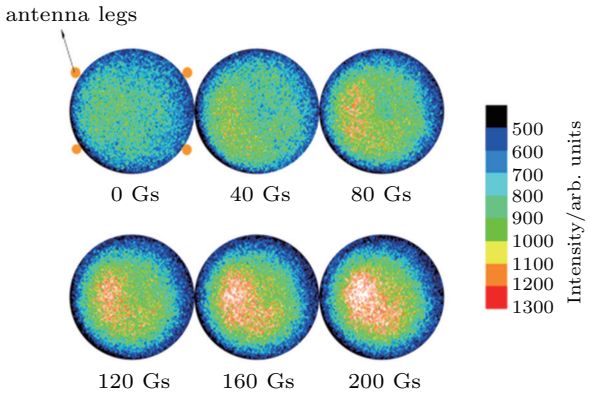


Fig. 3. (color online) End-viewed ICCD images for different $B_{\rm ex}$ values at a pressure of 0.35 Pa and an RF power of 140 W in Case 1.

The axial profiles of electron density along the discharge tube in different $B_{\rm ex}$ values are shown in Fig. 4(a). The higher density of electrons is located around the antenna when the external magnetic field is zero, but moves toward the upper half of the tube (i.e., $Z > 0$) as $B_{\rm ex}$ increases. The larger the magnetic field, the closer to the upper end-plate the high-density area is. The electron density in the upper half is almost identical at a level of $n_{\rm e} \approx 4 \times 10^{16}/{\rm m}^3$ when $B_{\rm ex}$ is large enough (> 100 Gs). The electron density is a little lower than the value indicated in Lafleur *et al.*'s work[8,13] due to a lower power and power density in this experiment. In addition the capacitive discharge may also play a role in the case of low power which leads to a lower electron density.

Figure 4(b) shows the distributions of electron temperature ($T_{\rm e}$) along the axis at different $B_{\rm ex}$ values. Like the electron density case in Fig. 4(a), $T_{\rm e}$ is also higher in the upper

half of the tube at all B_{ex} values. The external magnetic field can only change the motion directions of electrons into the direction perpendicular to the magnetic direction and it does not affect the electron motion in the parallel direction, so the variations of electron density and temperature along the axis will not be caused by the magnetic confinement of plasma. Instead, it comes from the bulk absorption in helicon wave that increases the density and temperature at the same time. According to the dispersion relationship of the helicon wave, the electron density increases with magnetic field increasing. The plasma is therefore expected to be denser in the upper half of the tube than in the bottom half.

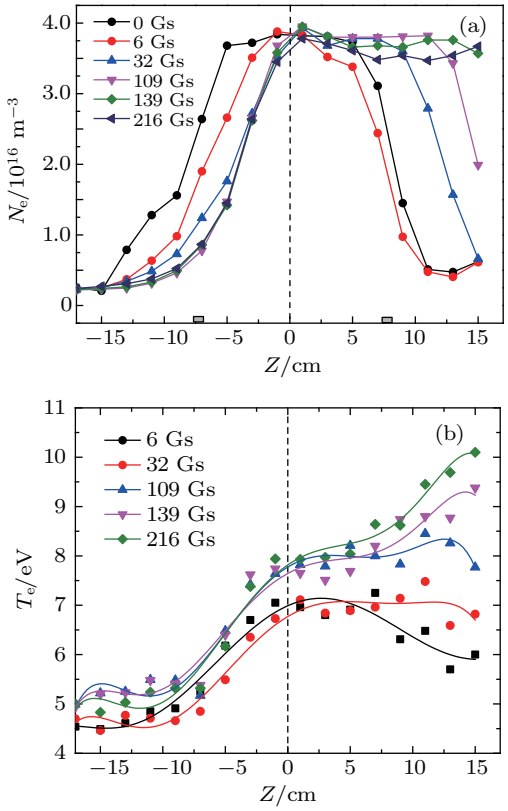


Fig. 4. (color online) Tube-axial profiles of (a) electron density and (b) electron temperature in Case 1 at different B_{ex} values.

To confirm this hypothesis, we then diagnose the electromagnetic signals by B-dot probe measurement. The probe is positioned at the symmetrical axis of the azimuthal antenna straps to avoid interference by the field in the near-field region of the antenna.[28] At the same time the field in the near-field region of RF coil is small enough so that it cannot have much influence on the results of helicon waves. Figure 5 shows the variations of axial profile of the amplitude and phase of B_z in the discharge tube (or source region) where $r = 2$ cm. The RF current in the antenna is simultaneously measured by a Rogowski coil as a phase reference.

As seen in Fig. 5, as the magnetic field increases, the standing wave is formed in most parts of the tube, while the traveling wave is formed near the upper end. It means that the traveling wave causes the luminance to concentrate around the axis. In Case 1 the discharge is mainly caused by the traveling helicon wave. The traveling helicon wave propagates along the plasma column in the upper half of the tube and deposits energy though a variety of absorptions such as collisions, Landau damping, and/or trapping of electrons.[29] These energy delivery types are undertaken in a competitive manner, and one or a few RF powers are chosen to deposit energy into the plasma finally. Kamenski and Borg[30] suggested that linear energy absorption plays a main role in high density plasma while the nonlinear energy deposition model plays a main role in low density.

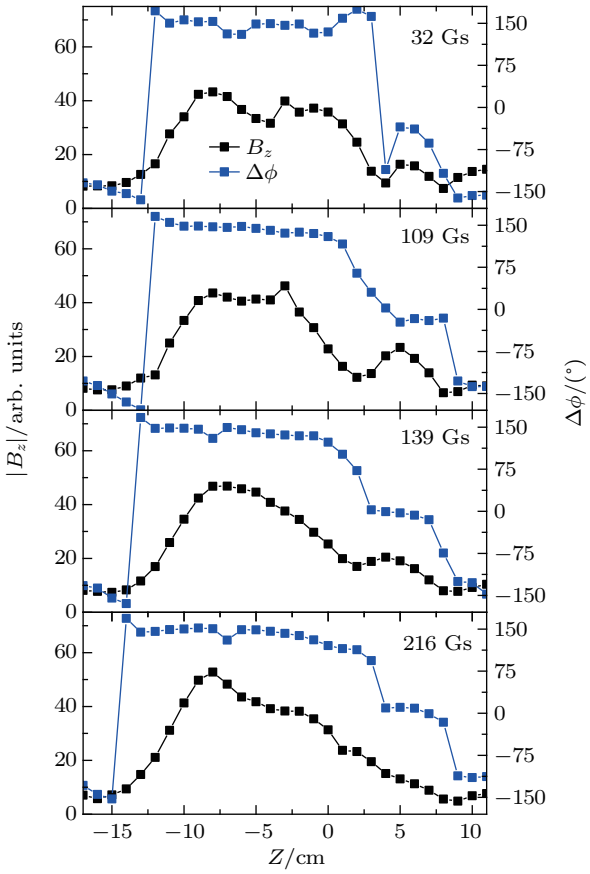


Fig. 5. (color online) Axial profiles of the amplitude and phase of B_z in the discharge tube where $r = 2$ cm when the supply power is 140 W.

3.2. Case 2: B_{ex} located in the middle of antenna

Figure 6 shows the end-viewed ICCD images of the discharge in Case 2 with increasing magnetic field.

The radial glow distribution in Case 2 is completely different from in Case 1. One can see that the discharge becomes stronger as the magnetic field increases, and the intense luminance region moves to the edge of the tube. In most of the plasmas there is a central peak on axis no matter whether the plasmas are magnetized or unmagnetized due to a short-circuit effect at the endplates,[31] but it is not the case here. In fact, there are also some situations where the density is not peaked on the axis,[32] in which obvious ionization near the edge excited by Trivelpiece–Gould wave can be seen. The luminance

reaches the strongest value at $B_{ex} = 145$ Gs. As B_{ex} is further increased, the intense light becomes weaker and the glow moves to the two legs of the antenna. The discharge evolution with magnetic field increasing is very similar to that in the uniform magnetic field. In this case, the effective antenna resistance R_{eff} generally shows one peak as magnetic field B_{ex} increases as shown in Fig. 7. The position of the peak (around 145 Gs) is consistent with the scenario in the ICCD image. The position of R_{eff} peak depends on the RF power, shifting to 145 Gs at 140 W to 120 Gs at 100 W.

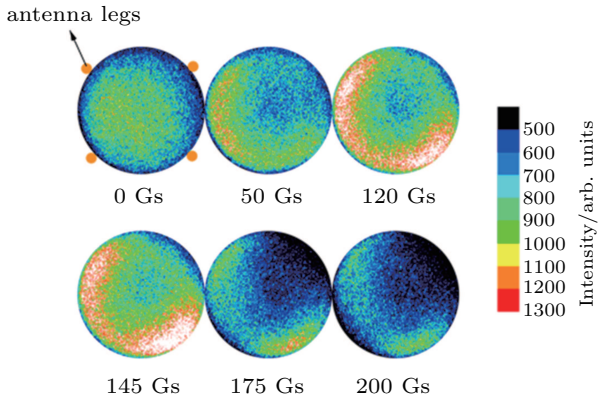


Fig. 6. (color online) End-viewed ICCD images in Case 2 at different magnetic field B_{ex} values when the working pressure is 0.35 Pa and RF power is 140 W.

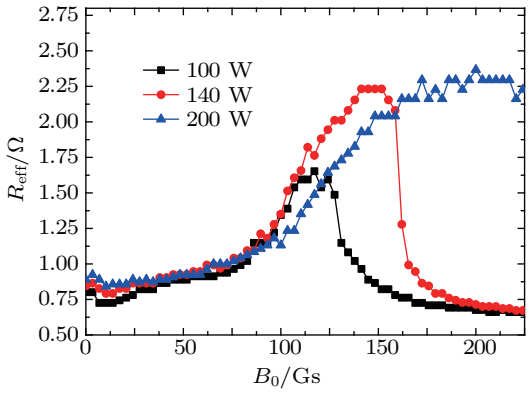


Fig. 7. (color online) Variations of effective resistance of antenna with magnetic field B_{ex} in Case 2 at different RF powers.

Figure 8(a) shows the axial profiles of electron density along the central axis of tube in Case 2 at different B_{ex} values. It is seen that the plasma is mainly centralized in the middle of the discharge tube ($Z = -7.5$ cm–7.5 cm), which is similar to that in the case of uniform magnetic field.[16] Figure 8(b) shows the axial profiles of electron temperature in different magnetic fields. One can see that T_e is relatively high in the middle of the tube.

The axial profiles of electron density (see Fig. 8) demonstrate that the power deposition mainly concentrates in the region near the antenna (-7.75 cm$< Z <$ 7.75 cm). Only one low-field peak exists with external magnetic field increasing in Fig. 7. This suggests that the helicon wave has only one wave number in the axial direction, with the wave number given, and the electron density will increase linearly with magnetic field increasing according to the dispersion relationship.[16] Therefore, we consider that the discharge in Case 2 is caused by TG-wave-induced surface mode conversion, even if the magnetic field is non-uniform. In the process of surface non- resonance mode conversion, the helicon wave can excite TG wave. The strongly damping TG wave leads to the energy absorption and discharge in this case.

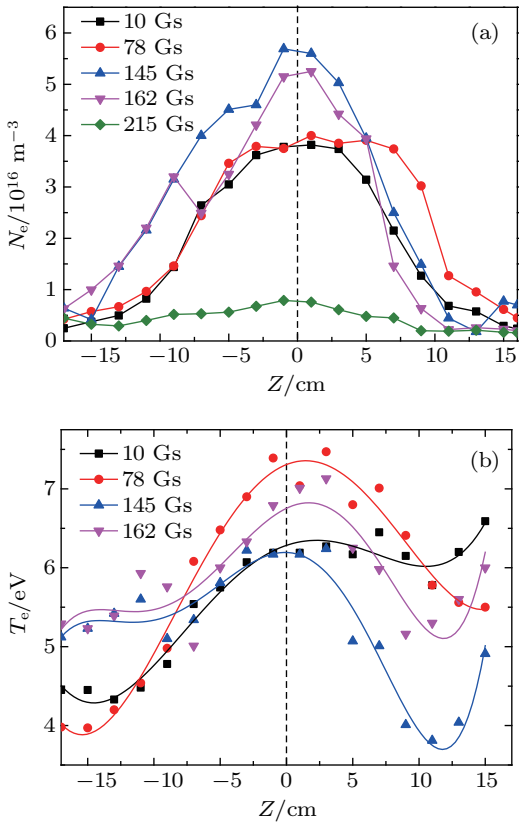


Fig. 8. (color online) Axial profiles of (a) electron density and (b) electron temperature along the discharge tube in Case 2 at different B_{ex} values and a 140-W RF power.

Figures 9 and 10 show the amplitudes and phases of B_z in diffusion chamber and the discharge tube in Case 2, respectively. It is seen in Fig. 9 that there is an amplitude peak of B_z at $Z = -22$ cm to -17 cm in the diffusion chamber when $B_{ex} = 145$ Gs, but there are almost no changes under the other magnetic fields. The linear increase of phase of B_z at $B_{0P} = 145$ Gs indicates the occurrence of the travelling wave. The calculated wave length ($\lambda = 360\mathrm{d}z/\mathrm{d}\phi$) is ~ 30 cm, which is about twice the antenna length (15.5 cm in the present work). In this condition there is a strong couple between the antenna and plasma, for a resistance peak appears at $B_{ex} = 145$ Gs as shown in Figs. 6 and 7.

In the discharge tube (or source region), standing waves form at the bottom half of the tube (see Fig. 10) in all tested magnetic fields. At the upper half, on the other hand, the helicon wave changes from standing wave into traveling wave, then turns back to standing wave as the magnetic field in-

creases. It is obvious that standing wave form always occupies the region of the antenna at all B_{ex} values.

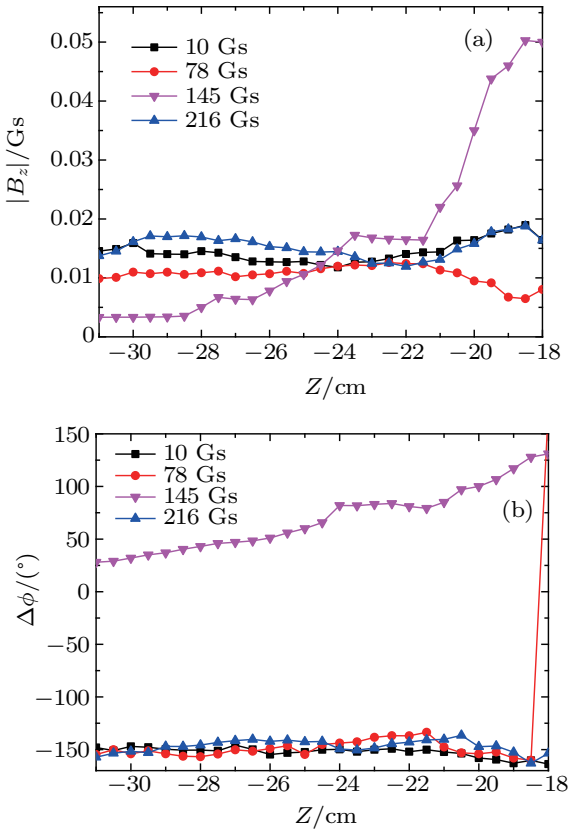


Fig. 9. (color online) Axial profiles of (a) amplitude and (b) phase of B_z in diffusion chamber in Case 2 at an RF power of 140 W.

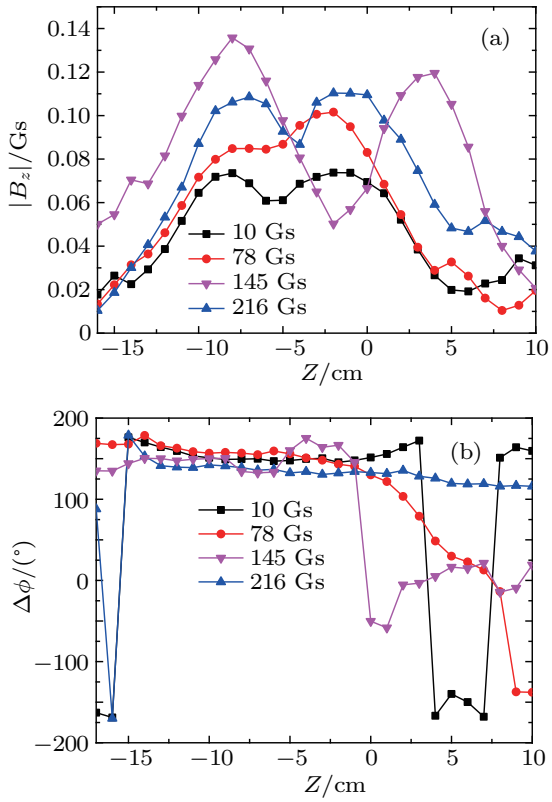


Fig. 10. (color online) Axial profiles of (a) amplitude and (b) phase of B_z in discharge tube in Case 2 at 140-W RF power.

In this case, all phenomena are similar to those in the uniform magnetic field. The effective resistance R_{eff} shows one peak with magnetic field B_{ex} increasing. The location of the peak shifts toward the higher magnetic direction with the RF power increasing (see Fig. 7). At the same time, most of RF power is deposited in the near region of the antenna. These results confirm that TG wave leads to energy absorption, and the TG wave is excited by the surface non-resonance conversion of helicon wave.[16]

3.3. Case 3: B_{ex} located at the tube end

Figure 11 shows the end-viewed ICCD images of the helicon discharge in Case 3.

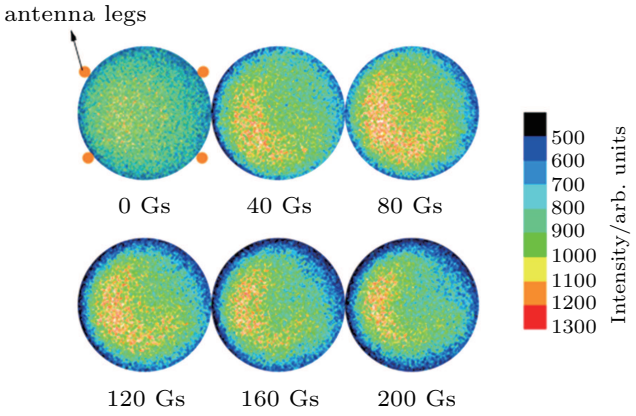


Fig. 11. (color online) End-viewed ICCD images in Case 3 at different values of magnetic field B_{ex}, a pressure of 0.35 Pa and an RF power of 140 W.

It is seen that the characteristic of discharge evolution at increasing magnetic field is similar to that of Case 1. The strongest luminance is located in the central region of the tube, and the radius of the strong luminance region increases with magnetic field. The difference is that the intensity of luminance in Case 3 is lower than that in Case 1, especially around the axis. But the effective resistance does not vary apparently with B_{ex}.

The axial profile of electron density in Case 3 at different values of B_{ex} is shown in Fig. 12(a). It is seen that the plasma prefers to be generated at the lower half of the tube. The distribution of T_e in Fig. 12(b) shows a similar tendency to the electron density. The T_e is higher in the bottom half than that in the upper half. The highest temperature region moves to the lower half of the tube when B_{ex} is larger than 52 Gs. These follow the profiles of the magnetic field.

The stronger magnetic-field component of the wave can still be centralized at the bottom of the tube and B_z will be kept in a constant phase with external magnetic field increasing as shown in Fig. 13. The standing wave is formed in most parts of the tube. In this case, the strongest discharge area is located at the lower half of the tube. This means that the standing wave plays a main role here. Hence the discharge region is close to the diffusion chamber instead of the end plate. This

may be the reason why there are similar discharge phenomena to Case 1 and Case 2, but different intensities and electromagnetic signals in discharge region.

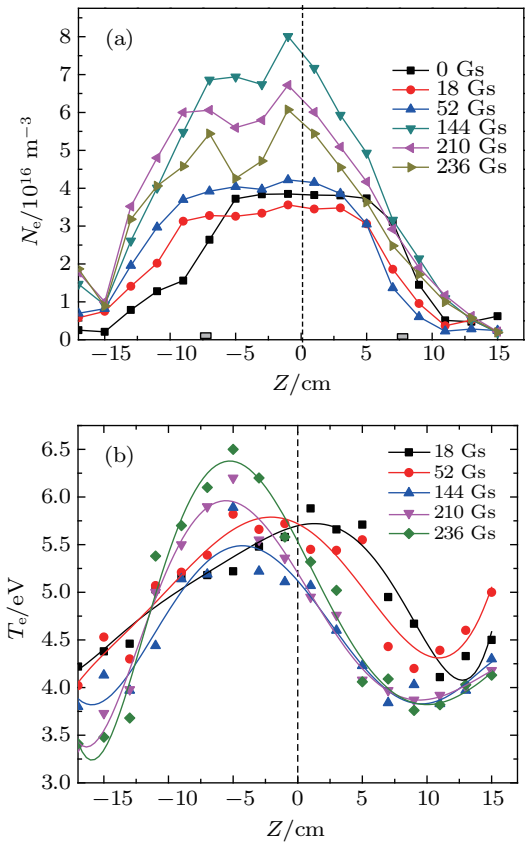


Fig. 12. (color online) Axial profiles of (a) electron density and (b) electron temperature in Case 3 at different B_{ex} values.

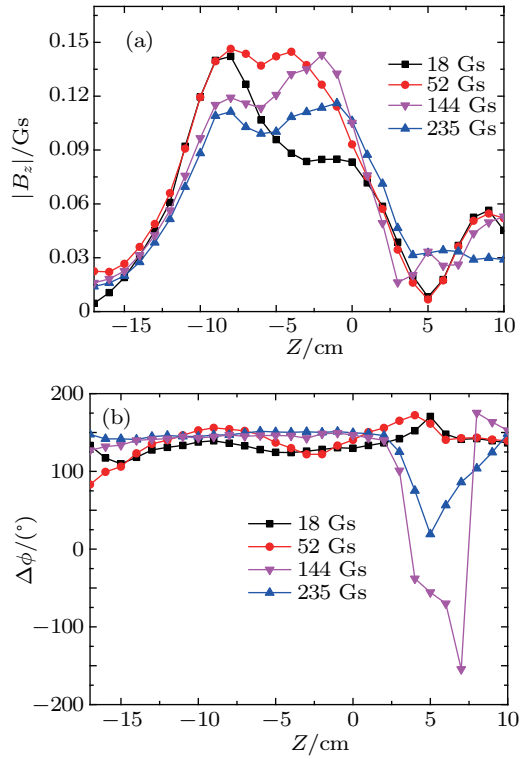


Fig. 13. (color online) Axial profiles of (a) amplitude and (b) phase of B_z in the discharge tube at $r = 2$ cm in Case 3 at a power of 140 W.

4. Discussion

As mentioned above, the electron density increases with magnetic field increasing according to the dispersion relationship of helicon wave. Most plasmas are generated at the upper half of the tube in Case 1, which infers that most RF power is mainly deposited at the upper half of the tube. Similarly, most RF power is deposited at the bottom half of the tube in Case 3. Since the TG wave can only be excited in the near region of the antenna, the helicon wave can propagate far away from the antenna. As a result, the plasma is generated around the axial line by the helicon wave. Unlike Case 1, the tube end in Case 3 contacts a diffused chamber. A bounded plate makes energy density higher and luminance stronger in Case 1 than in Case 3 with an unbounded boundary.

By considering the solution of helicon wave dispersion relationship, the helicon can only exist[14] under the condition of $\omega_{pe}^2/\omega_{ce}^2 N_{\parallel}^2 < 1/4$ and $\omega\omega_{ce}N_{\parallel}^2/\omega_{pe}^2 < 1$ (where m, e, and ω_{ce} are the electron mass, electron charge, electron gyro-frequency, and plasma frequency, respectively), and $N_{\parallel} = k_z c/\omega$ is the axial refractive index with k_z being the axial wave number. Thus, the helicon wave can propagate in the finite density range $n_{min} < n_e < n_{max}$, where $n_{min} = (\varepsilon_0 m/e^2)\omega\omega_{ce}N_{\parallel}^2$ and $n_{max} = (\varepsilon_0 m/4e^2)\omega_{ce}^2 N_{\parallel}^2$.

Since charged particles will be lost on the boundary, the electron density at the edge of the tube is smaller than in the case of bulk plasma, which can be confirmed by the distributions of the radial glow luminance in Figs. 3 and 11 (the electron density near the edge of the tube at $x \approx 3$ cm and $Z = 5$ cm is about 0.8×10^{10} cm^{-3}, but it is $\sim 3.9 \times 10^{10}$ cm^{-3} in the center at $x \approx 0$ and $Z = 5$ cm).

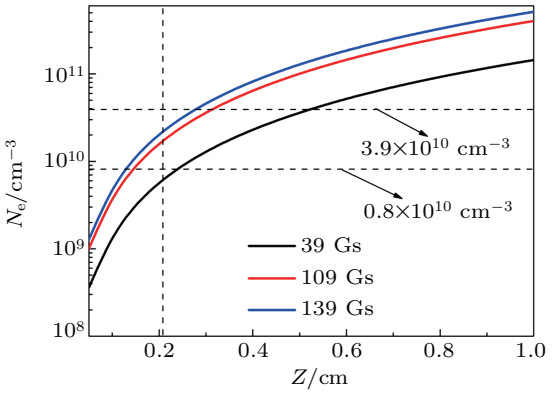


Fig. 14. (color online) Variations of electron density with axial wave number in different magnetic fields.

Figure 14 shows the variations of electron density with axial wave number at the values of magnetic field B_{ex} of 39 Gs, 109 Gs, and 139 Gs. The helicon wave only exists in the region above the curves shown in Fig. 14. Horizontal dashed lines show the plasma densities in the center ($N_e = 3.9 \times 10^{10}$ cm^{-3}) and the boundary ($N_e = 0.8 \times 10^{10}$ cm^{-3}), respectively. For an antenna with 15.5 cm in length, it prefers to excite a wave with a wavelength of 31 cm (i.e., twice the antenna length). We therefore concentrate on the propagation region of the helicon wave with an axial wavelength of 31 cm or $k_z = 0.203$ cm^{-1}.

From Fig. 14, one can find that the propagation region of helicon wave decreases as the magnetic field increases at the same electron density. As a result the luminous glow in radial cross section appears in Cases 1 and 3.

Power transfer efficiency η is one of the important parameters to describe the helicon discharge, which is defined as $\eta = R_{\rm p}/R_{\rm eff} = R_{\rm p}/(R_{\rm p}+R_{\rm A})$ (where $R_{\rm p}$ is the plasma resistance, $R_{\rm A}$ the antenna resistance and $R_{\rm eff}$ the effective resistance). A higher η corresponds to a higher ionization rate, and η has also a correlation with $R_{\rm eff}$. Then $R_{\rm eff}$ changes with the ionization rate and electron density. In Cases 1 and 3, $R_{\rm eff}$ does not vary apparently with $B_{\rm ex}$, but is kept around 0.8 Ω–1 Ω. In Case 2 there appears an $R_{\rm eff}$ peak with increasing external magnetic field (see Fig. 7). This indicates a higher efficiency in Case 2 than those in Cases 1 and 3. A peak of $R_{\rm eff}$ in Case 2 corresponding to high efficiency was also found by Lafleur *et al.*[21] Chen[33] also used the non-uniform change of plasma resistance to explain the jump of density. A high $R_{\rm eff}$ that is much larger than $R_{\rm A}$ means a very high efficiency η (close to 1). A higher loading (plasma) resistance is achievable with helicon plasma which turns into the RF absorption mechanism, which in helicon discharges is dominated by coupling to the rapidly damped TG mode.

It is noticed that there is always a standing wave forming near the antenna. Improvement of efficiency is accompanied by a traveling wave appearing in the region away from the antenna. The typical example is that a standing wave forms in the source region and a traveling wave forms in the diffusion chamber in Case 2 when $B_{\rm ex} = 145$ Gs. A similar electromagnetic behavior can also be found in the cases of larger power and higher magnetic field.[34] The standing wave may be due to the constructive interference between the forward wave and the reflected wave from the endplate.[10] This viewpoint can be verified by the work of Yang *et al.*[35] So it is proved that the nature of interference is a standing wave formed due to the superimposition of the helicon wave component and its back wave.

5. Conclusions

In this work, we investigate the characteristics of helicon wave plasma with different low axial magnetic field profiles in argon at 0.35 Pa. It is confirmed that the variation of axial low magnetic field profile can modulate the absorption manner. The electron density varies from 0.5×10^{16} m^{-3} to 9×10^{16} m^{-3} and the electron temperature ranges from 3 eV to 10 eV, which depends on magnetic field strength. When $B_{\rm ex}$ is located near the tube end sealed by a dielectric plate or near the diffusion chamber, the ICCD images show the strongest luminance located in the central region of the tube. The distributions of electron density and temperature along the Z axial direction in different external magnetic fields demonstrate that the helicon wave plays an important role. The type of end boundary makes the difference in the two cases. When $B_{\rm ex}$ is located in the middle of the antenna, the glow in radial cross section moves toward the edge of the tube and then toward the two antenna legs as the magnetic field is increased. In this case, an $R_{\rm eff}$ peak appears with increasing magnetic field. The location of the peak shifts toward higher magnetic field with power increasing. The strongly damping TG wave excited by the surface non-resonance mode can be used to explain these results. The effective resistance also shows that the energy transmitted by the TG wave excited by the helicon wave in the second profile of $B_{\rm ex}$ has a higher efficiency. The signal of the standing wave appears in all cases, which is formed by the superimposition of the helicon wave component and its back wave.

References

[1] Boswell R W 1970 *Phys. Lett. A* **33** 457
[2] Chen F F 2015 *Plasma Sources Sci. Technol.* **24** 014001
[3] Chen F F and Boswell R W 1997 *IEEE Trans. Plasma Sci.* **25** 1245
[4] Shamrai K P and Taranov V B 1996 *Plasma Sources Sci. Technol.* **5** 474
[5] Chen F F, Jiang X, Evans J D, Tynan G and Arnush D 1997 *Plasma Phys. Contr. Fusion* **39** A441
[6] Lho T, Hershkowitz N, Miller J, Steer W and Kim G H 1998 *Phys. Plasmas* **5** 3135
[7] Wang S J, Kwak J G, Kim C B and Kim S K 2003 *Phys. Lett. A* **313** 278
[8] Lafleur T, Charles C, and Boswell R W 2010 *Phys. Plasmas* **17** 073508
[9] Degeling A W, Jung C O, Boswell R W and Elingobe A R 1996 *Phys. Plasmas* **3** 2788
[10] Chen F F 2003 *Phys. Plasmas* **10** 2586
[11] Cho S 2006 *Phys. Plasmas* **13** 033504
[12] Sato G, Oohara O and Hatakeyama R 2007 *Plasma Source Sci. Technol.* **16** 734
[13] Lafleur T, Charles C and Boswell R W 2011 *Phys. Plasmas* **18** 043502
[14] Barada K K, Chattopadhyay P K, Ghosh J, Kumar S and Saxena Y C 2013 *Phys. Plasmas* **20** 042119
[15] Barada K K, Chattopadhyay P K, Ghosh J, Kumar S and Saxena Y C 2013 *Phys. Plasmas* **20** 012123
[16] Wang Y, Zhao G, Liu Z W, Ouyang J T and Chen Q 2015 *Phys. Plasmas* **22** 093507
[17] Lafleur T, Charles C and Boswell R W 2010 *Phys. Plasmas* **17** 043505
[18] Charles C and Boswell R W 2004 *Phys. Plasmas* **11** 1706
[19] Charles C and Boswell R W 2007 *Appl. Phys. Lett.* **91** 201505
[20] Virko V F, Shamrai K P, Virko Y V and Kirichenko G S 2004 *Phys. Plasmas* **11** 3888
[21] Lafleur T, Charles C and Boswell R W 2011 *J. Phys. D: Appl. Phys.* **44** 055202
[22] Takahashi K, Motomura T, Ando A, Kasashima Y, Kikunaga K, Uesugi F and Hara S 2014 *J. Phys. D: Appl. Phys.* **47** 425201
[23] Takahashi K, Takayama S, Komuro A and Ando A 2016 *Phys. Rev. Lett.* **116** 135001
[24] Boswell R W 1970 "A Study of Waves in Gaseous Plasmas", Ph D. Thesis (Flinders University)
[25] Sun B, Huo W G and Ding Z F 2012 *Rev. Sci. Instrum.* **83** 085112
[26] Chen F F 1991 *Plasma Phys. Control. Fusion* **33** 339
[27] Ganguli A, Sahu B B and Tarey R D 2007 *Phys. Plasmas* (1994–present) **14** 113503
[28] Shamrai K P 1998 *Plasma Sources Sci. Technol.* **7** 499
[29] Boswell R W and Chen F F 1997 *IEEE Trans. Plasma Sci.* **25** 1229
[30] Kamenski I V and Borg G G 1996 *Phys. Plasmas* **3** 4396
[31] Chen F F 2013 *Phys. Plasmas* **20** 057102
[32] Chen F F 2012 *Phys. Plasmas* **19** 093509
[33] Chen F F 2007 *Plasma Sources Sci. Technol.* **16** 593
[34] Niu C, Zhao G, Wang Y, Liu Z W and Chen Q 2017 *Phys. Plasmas* **24** 013518
[35] Yang X, Cheng M S, Wang M G, *et al.* 2017 *Acta Phys. Sin.* **66** 025201 (in Chinese)